Research Article Vol. 2, No. 10 / 15 October 2019 / OSA Continuum 2844

Experimental characterization of directional couplers in InP photonic membranes on silicon (IMOS)

ALI EMRE KAPLAN,[1,*] GAETANO BELLANCA,[1] JORN P. VAN ENGELEN,[2] YUQING JIAO,[2] JOS J. G. M. VAN DER TOL,[2] AND PAOLO BASSI[3]

[1]Department of Engineering, University of Ferrara, Via Saragat, 1, Ferrara, 44122, Italy
[2]Institute of Photonic Integration, Eindhoven University of Technology, Eindhoven 5600 MB, The Netherlands
[3]Department of Electrical, Electronic and Information Engineering, University of Bologna, Viale del Risorgimento, 2, Bologna, 40136, Italy
[*]aliemre.kaplan@unife.it

Abstract: We experimentally study the performance of directional couplers fabricated in indium-phosphide membrane on silicon (IMOS) technology. We both investigate the validity of the coupled mode theory (CMT) applied to directional coupler structures with high index contrast and study the effect of some different topological choices in device fabrication. In particular, besides the conventional curved structures, we consider ultra sharp corner bends that reduce the footprint. The effect of fabrication tolerances on the different guided mode polarizations is also discussed.

1. Introduction

Directional couplers (DCs) are one of the fundamental building blocks of photonic integrated circuits (PICs). They allow electromagnetic power exchange between two or more closely spaced waveguides. Typical applications of DCs are power splitting or wavelength filtering, as well as switching, if electrical controls are present. Design and characterization of such components is then crucial to exploit new functionalities and to conceive innovative devices for forthcoming applications such as, for example, the upcoming 5G infrastructure. In this scenario, the interplay among the design, the fabrication and the characterization steps has become even more important thanks to the expanding of the so called "Generic foundry approach" to PICs fabrication, based on either silicon or in indium-phosphide technologies (see for example [1–3]).

This approach allows users to design their own devices assembling the necessary building blocks only considering the desired functional behavior. The link between device functionality and technological parameters (materials, device geometries and foundry facilities) is provided by the so called Process Design Kits (PDK), a set of files modeling the fabrication process. The use of the PDK makes technological issues fully transparent to the designer and, above all, guarantees that the circuit performance fits the desired one. Setting up a PDK requires a preliminary intense activity to determine the relationships between the parameters to be inserted in the design equations and the technological ones, in order to obtain full correspondence between the expected and the measured device characteristics.

This paper aims at presenting some results of such activity performed on couplers realized with a new and promising technological approach, the IMOS technology. The interest in this platform comes from the possibility it allows to integrate active and passive components in the same chip [4]. The task of determining the functional parameters of such components is challenging. The use of a numerical approach would certainly lead to realistic answers, since

#371353 https://doi.org/10.1364/OSAC.2.002844
Journal © 2019 Received 4 Jul 2019; revised 31 Aug 2019; accepted 5 Sep 2019; published 26 Sep 2019

OSA CONTINUUM

any device can be precisely modeled even in 3D. However, this approach is not applicable in the proposed design process. It requires specific modeling of the considered devices while users should not be involved in this task, but limit their attention to the device functional behavior. So, in practice, analytical models should be set up, with characteristic parameters grasped integrating the results of many numerical simulations, fabrication runs and experimental measurements. This has renewed the interest for classic analytic approaches, revisited and used in the framework of the new experimental conditions. In the case of couplers, the Coupled Mode Theory (CMT) is obviously the natural choice.

This approach was originally formulated assuming some hypotheses on material and device features which are no longer valid for today's devices [5–14]. Its original formulation assumed in fact a small index contrast between core and cladding and weak waveguide coupling. These hypotheses were fully compatible with the available technology. But this is no longer true for integrated optics that uses high-index contrast materials technologies such as silicon-on-insulator (SOI) and IMOS. One can then question about the accuracy of the results obtained with this approach. In a recent paper it has been however shown how, even though a high index contrast is present, the CMT can still be successfully used [15]. That study stimulated the present work, which has then the twofold purpose of both comparing the CMT theoretical results with the experimental ones in the case of high index contrast waveguides, such as those obtained on the IMOS platform, and to assess the quality of this promising technological process.

The paper is structured as follows. In the next section, we introduce the fabricated and measured types of couplers and the design parameters that we used in this work. In section 3, the CMT and the fitting procedure main features will be illustrated. Section 4 will present the theoretical and experimental results. This will allow to discuss also the effect of fabrication tolerances for both transverse electric (TE) and transverse magnetic (TM) polarized input. Conclusions will be finally drawn.

2. Studied directional coupler structures

In the following we will consider directional couplers made by two parallel waveguides. In particular, two different types of DCs have been investigated. They are sketched in Fig. 1.

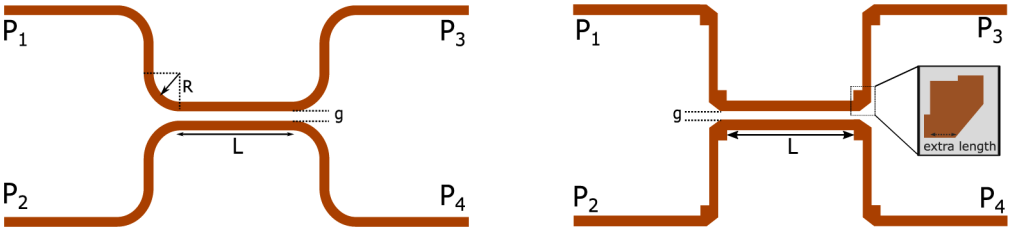

Fig. 1. Sketches of the two studied symmetric coupler structures: (a) with bends; (b) with mirrors. The corner bend is placed as an inset for showing the extra length to the coupling section.

The former structure (shown in part (a) of the figure) has the classical shape, with two parallel waveguides close enough to couple the desired amount of power from one waveguide to the other, and input and output sections made by curved bends. Both curves of each arm have radius R. Inevitably, some coupling occurs also in these bends. This affects the overall coupler performance. Though such undesired coupling decreases when R decreases, it cannot be fully eliminated, since too small values of R cause unwanted high radiation losses. It is then better to include this effect in the design procedure. This can be done simply increasing the real coupler

OSA CONTINUUM

length L by a further coupling length L_b that represents effective extra length resulting from the bend coupling. Alternatively a sharp corner with low loss can be made by a mirror [16] instead of bend, as sketched in part (b) of the same figure. This provides the advantage of further reduction of the circuit foot print. However, as shown by the inset of the figure, representing a corner, the mirror shape is in fact somehow complicated to reduce the overall device losses. So, also in this case, an extra coupling length L_b should be considered.

In both designs, the ports labeled as P_1 and P_2 are the input ports, while P_3 and P_4 are the output ones. The straight sections of the coupler, with length L, are spaced by a gap g.

Two set of devices with curved bends have been fabricated with R equal to 10 or 15 μm. This allowed to investigate the strength of the coupling contribution imposed by the curves. Values of R have been chosen large enough to limit bending loss and polarization conversion. The values of the gap g and the length L of the parallel waveguide sections of both type of couplers are summarized in Table 1. For each value of g, ranging from 100 nm to 400 nm, some values of the coupler length L are considered. This will allow to determine, fitting the experimental results, the value of the coupling length L_c, i.e. the distance necessary to ensure a complete power transfer from one guide to the other.

Table 1. Couplers design parameters.

g (nm)	L (μm)
100	5, 10, 15, 20
200	10, 20, 30, 40
300	15, 30, 45, 60
400	35, 70, 105, 140

In the next section, the theoretical model used to describe the device behavior and the fitting procedure used to extract the structure parameters from the measured results will be illustrated.

3. Theoretical model of the directional couplers

The schematic of the central part of both type of couplers is shown in Fig. 2a. The deep etched InP membrane core has 400 nm width and 300 nm height and is bonded on an adhesive polymer, divinylsiloxane-bis-benzocyclobutene (DVS-BCB), that is used for wafer bonding of Si and InP [4]. Fig. 2b shows the picture of one of the fabricated directional couplers. In this picture, the dark parts are the InP whereas the brighter parts correspond to 2 μm wide trenches of the BCB bonding layer. Light coupling from fiber to the single mode waveguides is allowed through focusing grating couplers placed at the ends of the waveguides and each grating can excite either a quasi-TE or a quasi-TM mode.

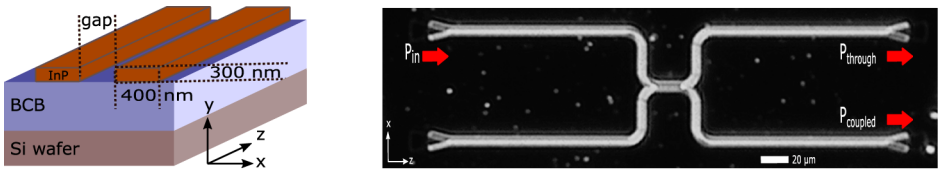

(a) (b)

Fig. 2. (a) Coupler structure schematic; (b) picture of a fabricated device.

The CMT model conventionally considers only the part of the device where the two waveguides are parallel and assumes that only one of the two input ports is excited by its guided mode. Using symbols introduced in Fig. 1 and normalizing powers so that $P_1(z = 0) = 1$ and $P_2(z = 0) = 0$,

OSA CONTINUUM

the two output powers are shown (see for example [5]) to be given by

$$P_3(z) = \cos^2(\kappa z) = P_t \tag{1}$$

$$P_4(z) = \sin^2(\kappa z) = P_c \tag{2}$$

where κ is the coupling strength and z is the longitudinal coordinate. P_t and P_c are also known as the *through* and *coupled* powers of the device. The distance at which coupling is complete is known as the coupling distance L_c. It depends on the coupling strength, described by the coupling coefficient κ. The relationship between L_c and κ can be found through the mismatch $\Delta\beta$, different for TE and TM polarizations, between the propagation constants of the two modes with even and odd symmetries of the full coupler, the so called device super-modes. It holds [17]:

$$L_c = \frac{\pi}{\Delta\beta} = \frac{\pi}{2\kappa}. \tag{3}$$

The CMT does not use super-modes, but computes the coupling coefficient using the modes of the single waveguides. Different expressions of κ have been proposed in these years, trying to adapt the original model to the new device features (higher index contrast, larger coupling, etc). In [15] some of the proposed CMT formulations have been checked to verify how successfully they can be used in the most demanding case of high index contrast and strong coupling, as it occurs in semiconductor waveguides. In particular, it has been shown that the coupling coefficient κ should consider not only the coupling between the transverse mode field distributions of the two single waveguides, but also between the no longer negligible longitudinal components. In other words, the coupling coefficient κ should be calculated as:

$$\kappa = \kappa^t + \kappa^z = \frac{\omega}{4}\int_{S_{\Delta\varepsilon}} \Delta\varepsilon\, \mathbf{E}_{t1}\cdot\mathbf{E}^*_{t2}\, dS + \frac{\omega}{4}\int_{S_{\Delta\varepsilon}} \Delta\varepsilon\, E_{z1}\, E^*_{z2}\, dS. \tag{4}$$

Superscripts t and z denote the transverse and longitudinal contributions due to the corresponding components of the electric field $\mathbf{E}$ of the two single parallel guides (named 1 and 2) and $\Delta\varepsilon$ is the dielectric constant perturbation that one guide introduces to the other to create the coupler. Values of (3), which can be considered exact, have been shown [15] to be in quite good agreement with those given by (4), while other expressions did not behave so well. All these values have been calculated using a Finite Element Method (FEM) mode solver [18].

The experimental check of the CMT model results requires however some further comment. In fact, as mentioned before, the simple model of parallel waveguides cannot be used to describe real structures. For example, the effect of the extra (variable) coupling due to transition regions (bends or mirrors) should be included in the equations. To do so, (1) and (2) have been rewritten as

$$P_{through} = \cos^2[\kappa(L + L_b)] \tag{5}$$

$$P_{coupled} = \sin^2[\kappa(L + L_b)] \tag{6}$$

where, as before, normalized powers $P_1 = 1$ and $P_2 = 0$ have been considered and κ is always the coupling coefficient given by the CMT. L is the length of the straight parallel waveguides (values listed in Table 1) while the extra coupling due to bends or mirrors has been then described by a fictitious length L_b, to be determined, which is added to the length L [19].

Moreover, the input and output powers depend also on the efficiencies of the input/output grating couplers and might perform differently device to device. In order to take into account

OSA CONTINUUM

also these effects, the measured output responses can be expressed as:

$$\left.\begin{aligned} P_{coupled_1} &= \sin^2[\kappa(L+L_b)]\cdot\alpha_1\cdot\alpha_4 \\ P_{through_1} &= \cos^2[\kappa(L+L_b)]\cdot\alpha_1\cdot\alpha_3 \end{aligned}\right\} \text{when } P_1 \text{ is considered as input} \tag{7}$$

and

$$\left.\begin{aligned} P_{coupled_2} &= \sin^2[\kappa(L+L_b)]\cdot\alpha_2\cdot\alpha_3 \\ P_{through_2} &= \cos^2[\kappa(L+L_b)]\cdot\alpha_2\cdot\alpha_4 \end{aligned}\right\} \text{when } P_2 \text{ is considered as input} \tag{8}$$

where α_i represents the overall attenuation induced by these effects in the i-th arm.

These four sets of measured data (two for each through and coupled ports) can be combined to eliminate the fiber-to-waveguide, bend and waveguide losses. One gets

$$\frac{P_t^2}{P_c^2} = \prod_{n=1}^{2}\frac{P_{through_n}}{P_{coupled_n}} = \frac{1-P_c^2}{P_c^2} = R' \tag{9}$$

where P_c and P_t have been defined by (1) and (2).

One can then finally get the set of values

$$P_c = \frac{1}{1+\sqrt{R'}} \tag{10}$$

which will be fitted by (6) to find κ and L_b.

In the next section, the couplers behavior will be studied only at the fixed wavelength $\lambda = 1550$ *nm*. Mode confinement and coupling strength depend in fact on wavelength and we did not want to consider also this further variable.

4. Experimental results and fitting procedure

In order to determine the coupler parameters and validate also experimentally the results obtained in [15], which suggest that Eq. (4) provides the best way to calculate the coupling coefficient κ to be used in the CMT, we have measured 96 devices (48 devices per polarization) fabricated with the design parameters reported in Table 1. The measurement setup is sketched in Fig. 3. Light from a tunable laser source is provided to an optical component tester. The output signal of the tester was used to excite the couplers (device under test, DUT) with the polarization adjusted by a polarization controller. The signal, guided by a SM fiber, is vertically coupled to the SM input waveguide of DUT via the on-chip grating couplers. The transmitted signal was then retrieved by a SM fiber connected to the tester to obtain the transfer function and monitored by the OSA using a splitter. Thermal stabilization of the chip during the experiments was done using a Peltier cell, driven by a temperature controller, placed under the aluminium chip holder.

The values of the parameters were found fitting the experimental results expressed by values given by (10) with those obtained by the theoretical model and given by (6). The fit process is critical for accurate interpretations of the experimental results. The fitting procedure to determine the values of κ and L_b was implemented by a MATLAB code [20]. Values of κ and L_b valid for each polarization have been determined applying a best fit procedure to each set of measurement results corresponding to couplers with the same shape and gap g, but different lengths L to find the best fitting values of κ (or, according to (3), L_c) and L_b. The initial guesses of κ and L_b were found to be crucial, since the error function had many local minima, but not all of them could be associated to physically reasonable results. In particular, as the extra coupling imposed by the bends can not be larger than the coupling resulting from an equi-length structure of parallel waveguides, L_b must be positive but also lower than the coupling length L_c. Moreover κ must

OSA CONTINUUM

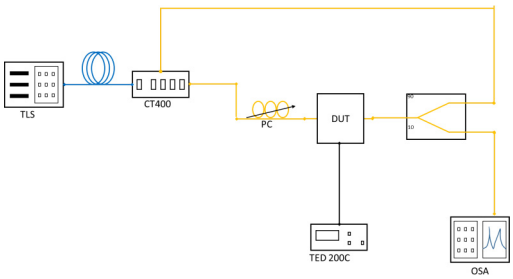

Fig. 3. Experimental setup for transmission measurements of the couplers. TLS: Tunable laser source (Yenista T100S-HP), CT400: Optical component Tester (Yenista CT400), TED 200C: Thermoelectric temperature controller (Thorlabs), OSA: Optical spectrum analyzer (Yokogawa AQ6370), DUT: Device under test and PC: Polarization controller.

decrease for increasing gaps. Considering these conditions, the optimization was implemented by making iterations of different initial guesses of κ and L_b. The expected values of κ were chosen using CMT while the maximum of expected values of L_b were normalized to L_c. Then, 20 iterations for κ were done by using $0.1 \cdot \kappa \cdot m$ where $m = 1, 2, 3, \ldots, 20$. and 10 iterations for L_b by $0.2 \cdot L_b \cdot n$ where, $n = 1, 2, 3, \ldots, 10$. Lastly, the local minimums of error function is inspected to check if it meets the conditions mentioned before. If not, this solution is discarded and new minimum of the error function is checked, until the all conditions are satisfied. As each iteration step for κ requires the whole set of iterations for L_b, so the total number of implemented iterations (200) was sufficient to provide full coverage of all possible fitted values according to the previously mentioned procedure conditions which can be listed as:

- The value of rmse of the fit function must be minimized.
- L_b obeys $0<L_b<L_c$.
- κ must decrease as the gap increases.

Figures 4 and 5 show respectively the results for the TE and the TM polarizations for different values of the gap g. Symbols refer to measured data and lines show the best fitting curves. Blue symbols or lines refer to devices with corner bends, the red color characterizes results obtained for devices with curved bends with 10 μm curvature radius, while green refers to devices with curved bends with 15 μm curvature radius. Part (a) of both figures refers to $g = 100$ nm, (b) refers to $g = 200$ nm, (c) refers to $g = 300$ nm and (d) refers to $g = 400$ nm. For a gap of 100 nm the effect of the extra coupling due to different transitions is evident. For larger gaps (and then longer devices) such effect tends to reduce. The overall standard deviation of rmse was found to be $4.6 \cdot 10^{-3}$.

An ideal DC coupler should have equally coupled powers independent from the input port. However, due to the measurement errors and possible imbalances in the upper and lower branches of the coupler (including total length and grating coupler performance), there can be some differences between the two measured coupled powers that can be defined as

$$\Delta P_c = \left| \frac{P_{coupled_1}}{P_{coupled_1} + P_{through_1}} - \frac{P_{coupled_2}}{P_{coupled_2} + P_{through_2}} \right|. \tag{11}$$

The error bars in Fig. 4 and Fig. 5 refer the mean value of a set of ΔP_c obtained from four measurements of each type of coupler (four different lengths for each gap). The small value of the standard deviation ($7.6 \cdot 10^{-3}$) of overall ΔP_c reasonably shows the repeatability of the measurements.

OSA CONTINUUM

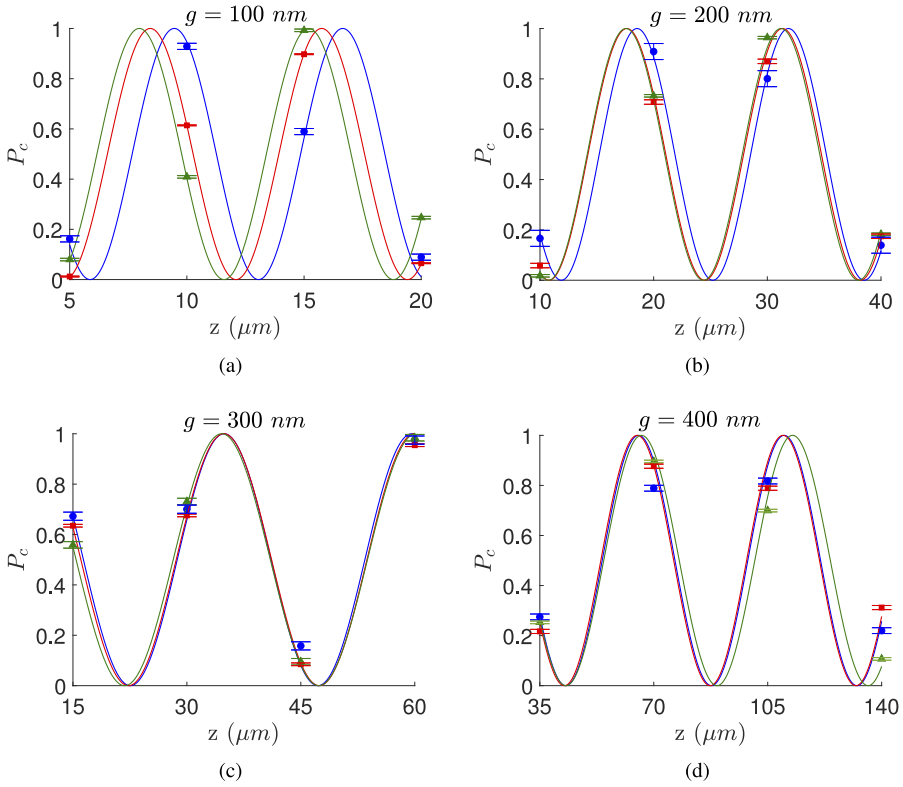

Fig. 4. Fit curves of measured P_c for TE polarized excitation of couplers with gap of (a) 100 *nm*, (b) 200 *nm*, (c) 300 *nm* and (d) 400 *nm*. Symbols refer to measured data, lines to best fitting curves. Blue refer to corner bends, red to curved bends with 10 μm curvature radius, green to curved bends with 15 μm curvature radius.

The fitting procedure allows to determine κ and then, once L_c has been calculated using (3), also to separate the bend contribution, given by L_b, which can be expressed introducing the parameter k_b defined by

$$k_b = \frac{L_b}{L_c}. \tag{12}$$

Values of k_b for the different configurations (bend radii of 10 and 15 μm and corner sections) are shown in Fig. 6. As expected, the weakest contribution comes from the corner bends, while larger curvatures contribute more to the total coupling. The negative trend of k_b for increasing gaps confirms also that bend contributions weakens for larger waveguide spacing. But even at larger gaps such as 400 *nm*, there is still some interaction between waveguides in both corner and curved bends. These results also confirm with that coupling of the TM polarization is stronger than that of the TE one.

More interesting results needing careful comments come from the fitted values of the coupling coefficients κ. These values are shown in Fig. 7. Symbols show the values obtained by the fitting procedure of the different structures, the dashed line shows the result of the CMT theory and the solid line shows those derived from super-mode simulations. One can note first that the symbols are always superimposed, i.e. that values of κ do not depend on the type of structure (bends or mirrors), which proves the quality of the fitting process. One can also see that the agreement between the experimental and the theoretical values of κ is much better for the TM polarized modes (Fig. 7b). Rather surprisingly, on the contrary, the coupling coefficients of TE coupler

OSA CONTINUUM

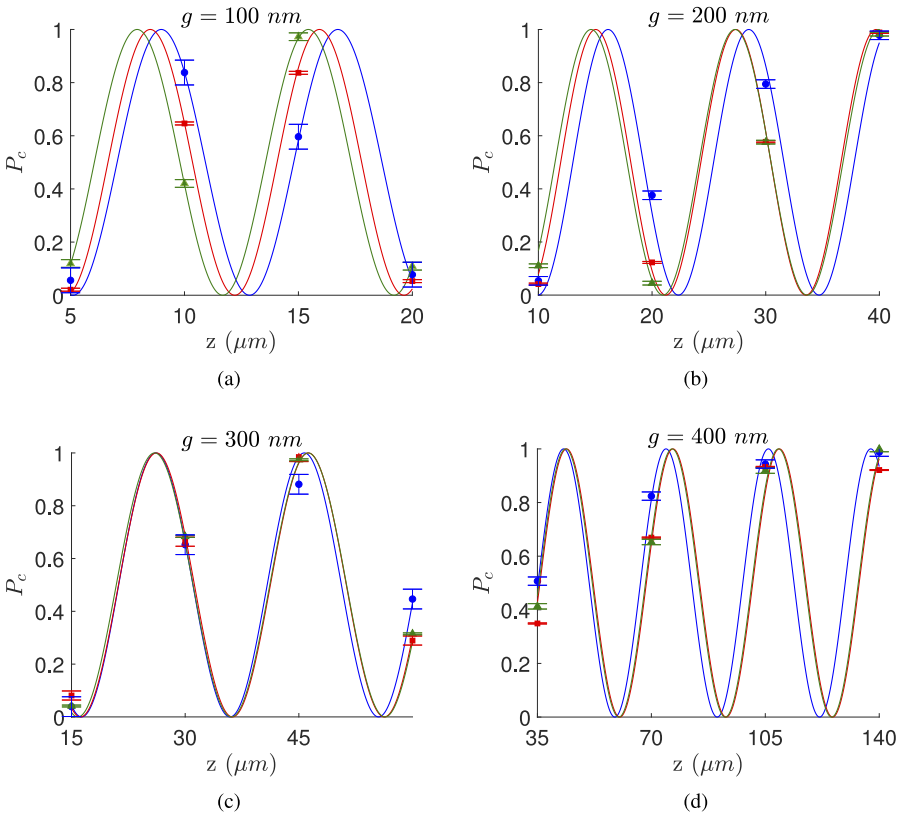

Fig. 5. Fit curves of measured P_c for TM polarized excitation of couplers with gap of (a) 100 *nm*, (b) 200 *nm*, (c) 300 *nm* and (d) 400 *nm*. Symbols refer to measured data, lines to best fitting curves. Blue refer to corner bends, red to curved bends with 10 μm curvature radius, green to curved bends with 15 μm curvature radius.

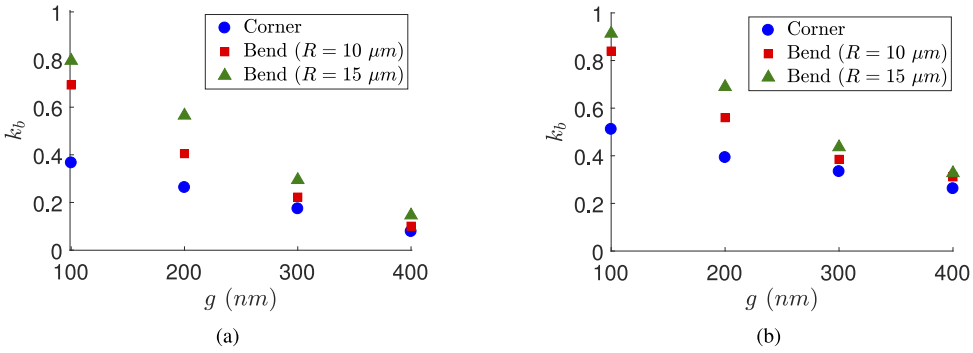

Fig. 6. Experimental results of bend coupling of TE (a) and TM (b) input polarization at $\lambda = 1550$ *nm*.

OSA CONTINUUM

are measured to be larger than the simulated ones (Fig. 7a). If we assume that both TE and TM couplers share the same fabrication tolerances, a possible reason of this mismatch can be related to some technological issues that can be more effective for TE polarized fields.

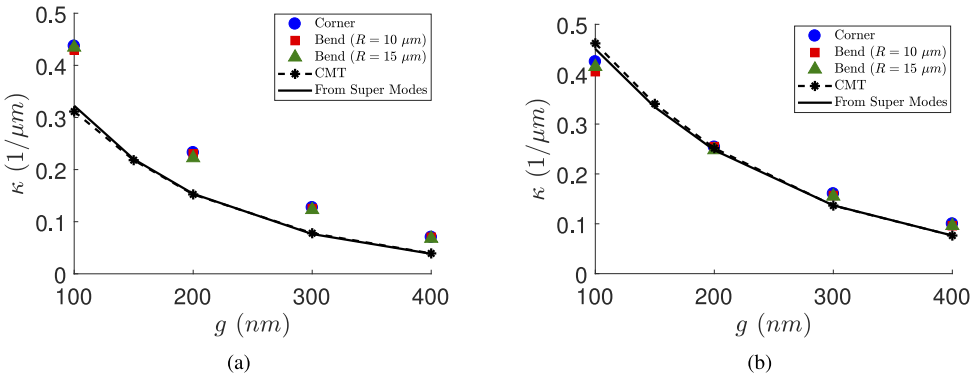

Fig. 7. Experimental results in comparison to FEM simulations of super-modes and Coupled Mode Theory for (a) TE and (b) TM coupling coefficient at $\lambda = 1550\ nm$.

To figure out the difference in expected and obtained results of the two polarizations, one can notice that the height of the waveguides is fixed with a good precision, since it depends on the layer thickness, which is precisely controlled. Their width, however, critically depends on the tolerances of the lithography process, which affect the lateral dimension, therefore, the gap. The different vertical and horizontal fabrication tolerances have an impact both on the mode shapes and on coupling. As the electric field is mostly horizontally polarized for TE modes and mostly vertically polarized for TM modes, the effect of fabrication errors in waveguide width and position should then impact more on TE than on TM modes.

A further technological issue to be considered comes from the etching process. Etching may for example induce some roughness in the waveguide sidewalls. This generates some scattering which affects coupling. But a larger effect is expected to come from the etching depth which can be due to the lag effect. Smaller gaps, in fact, reasonably make complete etching down to the required depth more difficult. For example, considering the topology with closest waveguide, the slot between the waveguides should be 300 *nm* deep and 100 *nm* wide.

To investigate the effect of all these possibilities (excluding scattering due to lateral surface roughness), we have then simulated different situations. We have changed the widths of the waveguides, the gap size, and added a floor in the slot, simulating a not perfect etching process. Parameter were changed one at a time, to check their relative effect on the final results. Values were chosen realistically, considering the used technology. The waveguide width tolerance was $\Delta w = \pm\ 20\ nm$, The footing layer was supposed to be up to 100 *nm* (irrespective of the gap, which is clearly a highly pessimistic hypothesis).

Figure 8 shows the width and etch depth (or footing layer) variations and results of post FEM simulations. The light blue areas represent the interval of the coupling coefficient for the worst cases of the gap and width combinations, related the E-beam lithography effects alone. Changes of the expected values of the coupling coefficients are small, but anyway explain rather well the discrepancies between the TM theoretical and experimental results. The (dark) grey areas refer on the contrary to the effect of the footing layer. This issue clearly affects mostly TE theoretical results. The decreasing difference between measured and expected values of the coupling coefficients confirms that the footing layer decreases for increasing gaps. The assumption of 100 *nm* thick footing layer was then pessimistic, but can be a starting point for a more detailed analysis.

OSA CONTINUUM

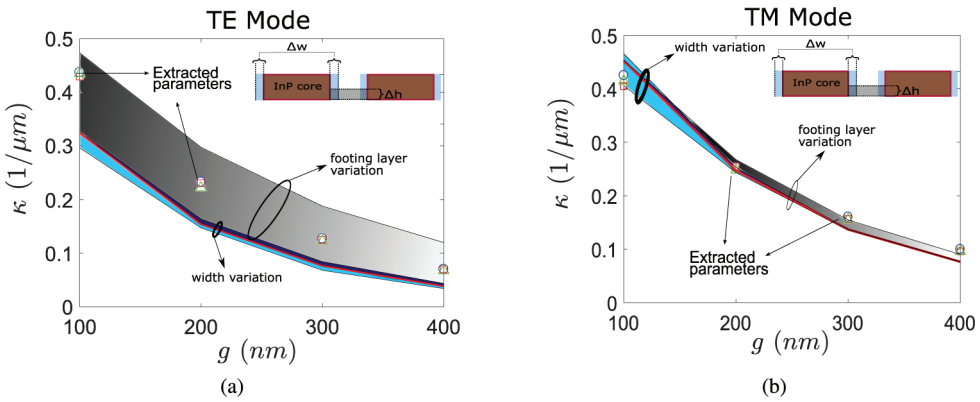

Fig. 8. The effect of fabrication variation on (a) TE and (b) TM mode coupling coefficient in terms of width ($\Delta w = \pm$ 20 *nm*), light blue domain and etch depth (Δh = 100 *nm*), grey domain. Red line represents the ideal case and dark blue parts are the cross section of width and etch depth variations. The cross section of coupler is placed as an inset.

As one can see, the introduction of the incomplete etch depth can reasonably explain the difference between measured and simulated coefficients for the TE polarized modes, suggesting that this is the most critical technological issue. Similarly, as previously reported in [21], TE coupling coefficients of shallow etched waveguides in SOI technology were mostly influenced by slab thickness variations while the effect of width variations were found to be weak. Correspondingly, we found similar results for deep etched waveguides. However, we additionally demonstrated that the effect of width variations, albeit limited, becomes dominant when a strong TM polarized coupling is present.

These results also allow to conclude that devices based on the TM polarized modes have the advantage of being more tolerant to fabrication issues as their performance depends more on the membrane thickness, which is precisely controlled. However, since the TE modes are more confined in the guide, bends with smaller radius for TE mode are allowed and provide lower bend losses.

5. Conclusion

In this paper we have presented a theoretical and experimental analysis of directional couplers with both curved and corner bend connectors, fabricated by the IMOS technology aiming both at experimentally assessing the CMT and defining design criteria to set up design kits for this recent and promising technology. Key design parameters have been presented.

It has been first confirmed that corner sections have reduced coupling contributions and footprint compared to curved couplers. However, even if the waveguides are far from each other, there is always a non negligible coupling imposed by the corner sections.

We have then compared the TE and TM mode results in terms of coupling coefficient obtained by fitting the coupling ratio measurements. Neglecting the side-wall roughness effects, TM mode couplers exhibited an anyway good agreement between theoretical and experimental results, confirming the successful possibility of using the CMT theory also for high index contrast waveguides.

Larger discrepancies between theoretical and experimental results for the TE case have also suggested that a critical issue in device fabrication comes from the etching process, which does not allow complete etching for narrow trenches.

Finally, TM coupling coefficients were found to be more tolerant to fabrication variations than TE ones under the same deviations of waveguide width and etch depth in the coupling section.

OSA CONTINUUM

Acknowledgments

The authors acknowledge the Nanolab@TU/e cleanroom facility for the device fabrication. Gaetano Bellanca gratefully acknowledges support from "Bando per l'acquisizione di strumenti per la ricerca di Ateneo - Anno 2015" of the University of Ferrara.

References

1. M. Smit, J. J. G. M. van der Tol, and M. Hill, "Moore's law in photonics," Laser Photonics Rev. **6**(1), 1–13 (2012).
2. A. Eu-Jin Lim, J. Song, Q. Fang, C. Li, X. Tu, N. Duan, K. Kiong Chen, R. Poh-Cher Tern, and T. Liow, "Review of silicon photonics foundry efforts," IEEE J. Sel. Top. Quantum Electron. **20**(4), 405–416 (2014).
3. M. K. Smit, X. Leijtens, H. Ambrosius, E. Bente, J. van der Tol, B. Smalbrugge, T. de Vries, E.-J. Geluk, J. Bolk, R. van Veldhoven, L. Augustin, P. Thijs, D. D'Agostino, H. Rabbani, K. Lawniczuk, S. Stopinski, S. Tahvili, A. Corradi, E. Kleijn, D. Dzibrou, M. Felicetti, E. Bitincka, V. Moskalenko, J. Zhao, R. Santos, G. Gilardi, W. Yao, K. Williams, P. Stabile, P. Kuindersma, J. Pello, S. Bhat, Y. Jiao, D. Heiss, G. Roelkens, M. Wale, P. Firth, F. Soares, N. Grote, M. Schell, H. Debregeas, M. Achouche, J.-L. Gentner, A. Bakker, T. Korthorst, D. Gallagher, A. Dabbs, A. Melloni, F. Morichetti, D. Melati, A. Wonfor, R. Penty, R. Broeke, B. Musk, and D. Robbins, "An introduction to InP-based generic integration technology," Semicond. Sci. Technol.**29**(8), 083001 (2014).
4. J. J. G. van der Tol, Y. Jiao, L. Shen, A. Millan-Mejia, V. Pogoretskii, J. P. van Engelen, and M. K. Smit, "Indium phosphide integrated photonics in membranes," IEEE J. Sel. Top. Quantum Electron. **24**(1), 1–9 (2018).
5. E. A. J. Marcatili, "Dielectric rectangular waveguide and directional coupler for integrated optics," The Bell Syst. Tech. J. **48**(7), 2071–2102 (1969).
6. D. Marcuse, "The coupling of degenerate modes in two parallel dielectric waveguides," The Bell Syst. Tech. J. **50**(6), 1791–1816 (1971).
7. A. Yariv, "Coupled-mode theory for guided-wave optics," IEEE J. Quantum Electron. **9**(9), 919–933 (1973).
8. H. Kogelnik and R. Schmidt, "Switched directional couplers with alternating $\Delta\beta$," IEEE J. Quantum Electron. **12**(7), 396–401 (1976).
9. R. Schmidt and R. Alferness, "Directional coupler switches, modulators, and filters using alternating $\Delta\beta$ techniques (invited paper)," IEEE Trans. Circuits Syst. **26**(12), 1099–1108 (1979).
10. H. Haus and C. Fonstad, "Three-waveguide couplers for improved sampling and filtering," IEEE J. Quantum Electron. **17**(12), 2321–2325 (1981).
11. H. A. Haus and W. Huang, "Coupled-mode theory," Proc. IEEE **79**(10), 1505–1518 (1991).
12. A. Takagi, K. Jinguji, and M. Kawachi, "Wavelength characteristics of (2*2) optical channel-type directional couplers with symmetric or nonsymmetric coupling structures," J. Lightwave Technol. **10**(6), 735–746 (1992).
13. W.-P. Huang, "Coupled-mode theory for optical waveguides: an overview," J. Opt. Soc. Am. A **11**(3), 963–983 (1994).
14. Chang-Min Kim and Young-Joon Im, "Switching operations of three-waveguide optical switches," IEEE J. Sel. Top. Quantum Electron. **6**(1), 170–174 (2000).
15. G. Bellanca, P. Orlandi, and P. Bassi, "Assessment of the orthogonal and non-orthogonal coupled-mode theory for parallel optical waveguide couplers," J. Opt. Soc. Am. A **35**(4), 577–585 (2018).
16. Y. Jiao, J. Liu, A. M. Mejia, L. Shen, and J. van der Tol, "Ultra-sharp and highly tolerant waveguide bends for inp photonic membrane circuits," IEEE Photonics Technol. Lett. **28**(15), 1637–1640 (2016).
17. R. G. Hunsperger, *Integrated Optics*, 5th ed. (Springer, 2013), chap. 8.
18. COMSOL Multiphysics, https://www.comsol.com.
19. L. Chrostowski and M. Hochberg, *Silicon Photonics Design: From Devices to Systems* (Cambridge University Press, 2015).
20. The MathWorks, https://www.mathworks.com.
21. A. Prinzen, M. Waldow, and H. Kurz, "Fabrication tolerances of soi based directional couplers and ring resonators," Opt. Express **21**(14), 17212–17220 (2013).